ELSEVIER

Thermochimica Acta 289 (1996) 267–302

thermochimica acta

Development of a mathematical model and a simulator for the analysis and optimisation of batch reactors: Experimental model characterisation using a reaction calorimeter [1]

J.M. Zaldívar *, H. Hernández, C. Barcons

Joint Research Centre of the Commission of the European Communities, Institute for Safety Technology, Process Engineering Division TP680, 21020 Ispra (VA), Italy

Received 20 November; accepted 22 March 1996

Abstract

The mathematical modelling of a bench-scale batch reactor is presented. The formulation of the mass and heat balances leads to a set of algebraic-differential equations which, when solved, produce the temperature and concentration profiles as a function of time. Emphasis has been placed on a realistic description of such a reactor by incorporating an accurate representation of the heat effects, such as the heat taken by the reactor wall, heat losses, stirring power supply, heat of dilution, vortex influence on heat transfer area, and a model of the heating/cooling circuits as well as their controllers.

To obtain the data necessary to simulate the dynamic behaviour of the reactor, a set of characterisation tests was carried out. Once the different parameters of the model were evaluated, some experiments were performed to compare with the predicted dynamic behaviour obtained with the simulator. These experiments invluded the heating/cooling dynamic behaviour with different fluids, and the neutralisation reaction between sodium hydroxide and hydrogen chloride.

Keywords: Batch reactors; Mathematical modelling; Numerical simulation; Reaction calorimetry

* Corresponding author.

[1] This paper is a contribution to the special thematic issue "Reaction Calorimetry", edited by Ralph N. Landau.

PII S0040-6031(96)03023-7

List of symbols

A	frequency factor, depends on kinetics
A_L	set of chemical components
AQ	flow actuator
AT	temperature actuator
B	control signal for reactant feeds, dimensionless
c	molar concentration kmol m^{-3}
C_p	specifc heat capacity J kg^{-1} K^{-1}
C_{pL}	molar heat capacity of a chemical component J mol^{-1} K^{-1}
D	diameter m
e	thickness m
F	molar flow mol s^{-1}
h	partial heat transfer coefficient W m^{-2} K^{-1}
H	height m
K	coefficient of heat losses W K^{-1}
L	relative apparent molar enthalpy J mol^{-1}
Na	stirrer speed s^{-1}
N_E	number of reactant feed streams
N_L	number of liquid components
N_R	number of independent reactions
n	molar hold-up mol
Q	volumetric flow m^3 s^{-1}
QC	flow controller
r	rate of reaction mol l^{-1} s^{-1}
R	rate of chemical production or consumption mol l^{-1} s^{-1}
R	radius m
S	surface m^2
T	temperature K
TC	temperature controller
TM	temperature measurement
U	overall heat transfer coefficient W m^{-2} K^{-1}
US	effective heat transfer coefficient W K^{-1}
v	molar volume m^3 $kmol^{-1}$
V	volume m^3
WM	weight measurement
x	molar fraction or fraction of wetted heat exchange surface

Greek symbols

α	constant in stirrer power correlation, eqs. (54) and (55)
ΔH	enthalpy of reaction J mol^{-1}
ϕ	thermal flow W
Γ	thermal capacity J K^{-1}
η	dynamic viscosity Pa s

λ	thermal conductivity W m^{-1} K^{-1}
ν	stoichiometric coefficient, reactant(−), product(+) partial order or reaction
θ	parameter of a heat transfer correlation
ρ	density/kg/m^{-3}
τ	time constant/s
ψ	correction factor for the heat exchange model

Subscripts

0	reactor, internal side	ln	logarithmic average
1	reactor, external side	M	measurement
a	stirrer or ambient	m	reaction mixture
B	bottom	o	outlet
b	inserts	P	container heated loop
c	heat transfer fluid, cooled loop	p	pumps or proportional
d	dry part	r	reaction
dil	dilution	R	reactor
E	feed of reactants	r	radial
e	heat transfer fluid, heated loop	s p	set-point
h	heating	T	total
I	inlet or initial	t	hydraulic
k	cryostat	v	vortex
L	liquid	W	water
l	losses	w	wall or wetted part
lc	losses cooled loop	z	axial

Dimensionless groups

Fr	Froude number	$N_a^2 D_a g^{-1}$
Nu	Nusselt number	$U D \lambda^{-1}$
Pr	Prandtl number	$\eta C_p \lambda^{-1}$
Re	Reynolds number	$\rho_m Q D S^{-1} \eta^{-1}$
	for stirred tank	$\rho_m N_a D_a^2 \eta_m^{-1}$
Po	power number	$q_a \cdot \rho_m^{-1} N_a^{-3} D_a^{-5}$
S_k	shape factors	D_a/D_k (internal geometry)
V_i	Viscosity ratio	$\eta_{bulk}/\eta_{at\ wall}$

1. Introduction

The rapid development of the chemical industry in recent decades has increased the complexity of chemical plants, the diversity of products and the number of processes. This has produced a parallel increase in batch reactors, which due to their versatility allow the production of special chemicals (with very good yields, in small amounts,

when compared to those of continuous processes) and permit a rapid change from one process to other with minor modifications.

Unfortunately, the study of accident case histories [1] shows that batch units are usually more frequently involved in accidents than continuous process plants. These results are not surprising because batch processes are usually very complex, with reaction systems that normally are not entirely known; they also have strongly non-linear dynamics and their parameters vary with time. Furthermore, the fact that in a batch cycle there is no steady state implies that the operator must perform continuous corrections to control the process.

It has been argued that due to the small production levels, time constraints and the enormous variety of processes, the understanding of reactor dynamic behaviour is usually not economically justified. However, there are a considerable number of advantages. The most important is the optimisation of such processes. Such optimisation should take into account two different aspects: performance and safety. From the performance point of view, the optimal process design must allow the manufacture of products with the desired specifications in the minimum amount of time and with low operating costs. From the safety point of view, optimum process design must significantly reduce the risk of thermal runaway, avoiding intermediate accumulation of hazardous compounds and reducing the effects of cooling system malfunction or agitation stoppage. Obviously, the ideal situations would be those in which the process is inherently safe [2], i.e. where no disturbances whatsoever can cause an incident.

Mathematical modelling and dynamic simulation applied to these processes have been demonstrated to be very useful tools to obtain optimal yields [3] and to carry out thermal assessment [4]. However, this type of applications has been performed mainly for specific reactions in which the thermo-kinetic model was well known. In recent years, due to the fast development of digital computers, on-line identification applications have appeared [5]. These applications are based on the fact that, normally, the possibilities to optimise and control this type of reactor are limited, because of the uncertainties that allow few state variables or parameters to be measured, and amongst these only a few have sufficient time in advance to be incorporated in the control or/and decision chains. However, if by some procedre, i.e. estimation techniques, the state variables and fundamental parameters can be inferred, these new data can be used to perform predictive calculations about the future behaviour of the system, to detect in advance dangerous situations, to improve the control algorithms, and to assist the plant operators in their decisions about the correct measures to be adopted under certain situations.

In any case, a detailed dynamic model of the reactor, its accessories and its control system is a necessary prerequisite. Moreover, to achieve an understanding of the basic phenomena involved, it is vital to study simultaneously three different areas: the thermo-kinetics occurring in the reaction mixture, its interaction with the equipment, and the influence of the operating conditions.

The present investigation was undertaken with the main purpose of studying the dynamic behaviour and the influence of the initial and operating conditions in batch processes. To achieve this, a numerical simulator of a batch reactor has been developed. This model has been formulated and characterised experimentally using a commercial

bench-scale reactor [6]. Furthermore, the simulator was intended to serve as an aid to experiment design [7] and data analysis [8–10], allowing the determination of the optimal and safe operating conditions.

1.1. Generalities

The bench-scale reactor [6] under consideration is described in Fig. 1. The principal elements included in the simulator are indicated: the reactor vessel, the heating/cooling circuits, the feeding device and the controllers.

The description of the mathematical model is divided into three parts: the fundamental equations obtained from mass and energy balances, and equilibrium relations; the thermo-kinetic models introduced in these equations; and the model of the heating/cooling circuits and the feeding device.

The basic mathematical model considers a general case with the following characteristis:

- Operating mode:
  - Batch or semibatch with any number of feeding streams.
  - Adiabatic, isothermic, isoperibolic or temperature-programme modes.
- Chemical reactions:
  - Any number, taking place only in the liquid mixture.
  - Homogeneous or heterogeneous liquid–liquid reactions [11,12].
  - Irreversible, instantaneous or equilibrium types.
- Reactive mixture homogeneous or uniform for liquid–liquid systems.
- Heat effects:
  - Non homogeneous reactor wall.
  - Dynamics of the heating/cooling circuit.
  - Exchange with the surroundings including losses and stirring supply.

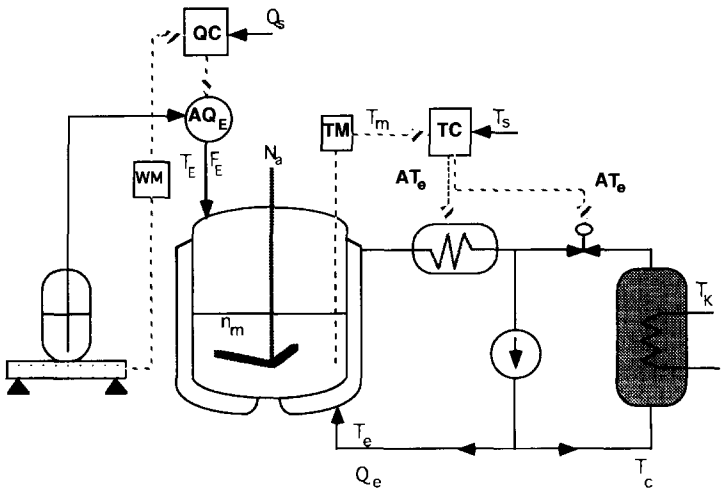

Fig. 1. Schematic representation of the bench-scale reactor.

1.2. Approach

The following criteria were taken into account in the design of the simulator:

- A compromise between the phenomena complexity and the model representability. Nevertheless, it must be able to represent the influences of all the relevant operating conditions, to model the control functions and reactor accessories.
- A coherence between the level of knowledge of processes: availability, accuracy, and validity range of data, and the simulator input.
- A flexibility from a physico-chemical point of view in order to deal with the diversity of substances and processes carried out in a batch reactor.
- A user-friendly and practical tool. As far as possible, it has to reproduce the functions of a real simulator: identity of task, control, and information generated.

2. Fundamental equations

Formulation of mass and energy balances for the reaction mixture provides the time-profile of the amount of each component present in the reaction mass and the temperature

$$\frac{\mathrm{d}n_{\mathrm{m}j}}{\mathrm{d}t} = F_{\mathrm{E}_j} + R_j V_{\mathrm{m}}; j \in A_{\mathrm{L}}(N_{\mathrm{L}}) \tag{1}$$

$$\frac{\mathrm{d}T_{\mathrm{m}}}{\mathrm{d}t} = \frac{1}{\Gamma_{\mathrm{m}}}(\phi_r + \phi_{\mathrm{E}} + \phi_{\mathrm{dil}} + \phi_{0_w} + \phi_{0_d} + \phi_{\mathrm{a}} + \phi_{\mathrm{l}}) \tag{2}$$

where the different heat flow rates included are:

ϕ_{r}, released by chemical reaction;
ϕ_{E}, due to mass addition;
ϕ_{dil}, due to heat of dilution of components;
ϕ_{0}, exchanged with the heat transfer fluid (w refers to wetted and d stands for dry part);
ϕ_{a}, supplied by stirring;
ϕ_{l}, exchanged with the surroundings,

and Γ_{m} is the thermal capacity of the reaction mixture and wetted devices, i.e. stirrer, temperature sensor, etc.

Due to the importance of the effect of the reactor wall on the heat transfer from/to the reaction mixture, and in order to take into account the possibility of heat accumulation in the wall during fast transients, a complementary heat balance is formulated which considers axial (z) and radial (r) conduction into the wall [13] including the bottom surface to the cylindrical part

$$\frac{\delta T_{\mathrm{w}}}{\delta t} = \frac{\lambda_{\mathrm{w}}}{\Gamma_{\mathrm{w}}}\left[\frac{1}{r}\frac{\delta}{\delta r}\left(r\frac{\delta T_{\mathrm{w}}}{\delta r}\right) + \frac{\delta^2 T_{\mathrm{w}}}{\delta z^2}\right] \tag{3}$$

With the boundary conditions

$$\lambda_w \frac{dT_w}{dr}\bigg|_{r=R_0} = h_0(T_{0_w} - T_m) \tag{4}$$

$$\lambda_w \frac{dT_w}{dr}\bigg|_{r=R_1} = h_1(T_e - T_{1w}) \tag{5}$$

The partial differential Eq. (3) is discretised spatially in order to obtain a set of ordinary differential equations consistent with the rest of the model. The number of discretisation points was chosen after an experimental study of the dynamics of the heating/cooling circuits, thus taking into account its smallest time constant. The wall is divided axially in two parts according to the surface wetted by the reaction mixture, and radially in three equally spaced parts, as indicated in Fig. 2.

The obtained time-profile temperatures through the reactor wall are

— internal side, wetted part (T_{0w})

$$\frac{dT_{0w}}{dt} = \frac{4}{\Gamma_w}(\phi_{0w} - \phi_{w1} - \phi_{w3}) \tag{6}$$

— centre wall, wetted part (T_{w1})

$$\frac{dT_{w1}}{dt} = \frac{2}{\Gamma_w}(\phi_{w1} - \phi_{w4} - \phi_{w2}) \tag{7}$$

— external side, wetted part (T_{1w})

$$\frac{dT_{1w}}{dt} = \frac{4}{\Gamma_w}(\phi_{w2} - \phi_{w5} - \phi_{1w}) \tag{8}$$

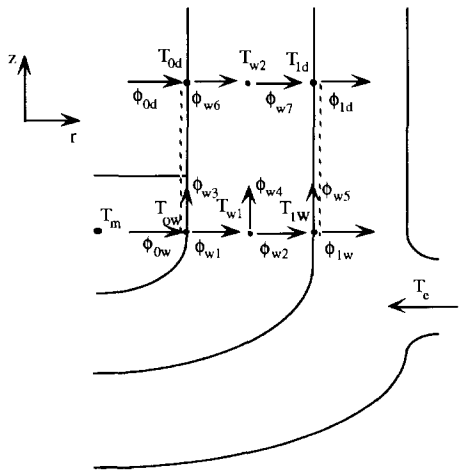

Fig. 2. Representation of the thermal fluxes and temperatures through the reactor wall.

— internal side, dry part (T_{0d})

$$\frac{dT_{0d}}{dt} = \frac{4}{\Gamma_d}(\phi_{0d} + \phi_{w3} - \phi_{w6}) \tag{9}$$

— centre wall, dry part (T_{w2})

$$\frac{dT_{w2}}{dt} = \frac{2}{\Gamma_d}(\phi_{w6} + \phi_{w4} - \phi_{w7}) \tag{10}$$

— external side, dry part (T_{1d})

$$\frac{dT_{1d}}{dt} = \frac{4}{\Gamma_d}(\phi_{w7} + \phi_{w5} - \phi_{1d}) \tag{11}$$

3. Thermo-kinetic models

From a calorimetric point of view, it is interesting to divide the thermo-kinetic phenomena according to their participation in the two main terms of the heat balance: heat production within the reaction mass, ϕ_{rxn}, and exchange of heat with the surroundings, ϕ_{ex}

$$\phi_{rxn} = \phi_r + \phi_{dil} \tag{12}$$

$$\phi_{ex} = \phi_{0w} + \phi_{0d} + \phi_1 + \phi_E + \phi_a \tag{13}$$

3.1. Heat production within the reaction mass

In this term are considered the enthalpy changes due to chemical reactions and physical phenomena taking place within the reactor contents, i.e. dilution, evaporation, etc.

The heat released by chemical reaction is calculated from the rates of reaction and their respective enthalpy changes. When the rate of reaction is defined per unit of mixture volume, the rate of heat generated is

$$\phi_r = V_m \sum_{i=1}^{N_r} (-\Delta H_i) r_i \tag{14}$$

where N_r is the number of independent chemical reactions.

Expressions for the rate of reaction, r, are defined in the most flexible way, in order to cover the diversity of cases. Reactions may be homogeneous or heterogeneous depending on the medium where they take place, or may be irreversible or instantaneous depending on the phenomena controlling the rate. The rate of reaction also allows the calculation of the net rate of transformation of each component, necessary to solve the mass balance

$$R_j = \sum_{i=1}^{N_r} \nu_{ij} r_i \tag{15}$$

The enthalpy change which accompanies the mixing or dilution of two or more substances is called the heat of dilution, and it may be calculated in the integral form as the change between the final and the initial state (before and after mixing) of the relative partial molar enthalpies multiplied by the number of mole of each component [14]. Thus

$$\Delta H_{\mathrm{dil}} = \sum_{k=1} \Delta(n_k L_k) \tag{16}$$

where n_k nad L_k are the number of moles and the relative apparent molar enthalpy of the kth component, respectively.

In order to obtain the rate of heat generation due to dilution, it is necessary to consider a differential change with respect to time of the heat of dilution [15]; hence

$$\phi_{\mathrm{dil}} = \frac{\mathrm{d}H_{\mathrm{dil}}}{\mathrm{d}t} = \sum_{k=1} \left(n_k \frac{\mathrm{d}L_k}{\mathrm{d}t} + L_k \frac{\mathrm{d}n_k}{\mathrm{d}t} \right) \tag{17}$$

3.2. Heat exchanged with the surroundings

The reaction mixture exchanges heat mainly with the heat transfer fluid that circulates in the jacket. The other terms considered in the heat balance are the enthalpy change due to mass addition, heat losses through the cover, and power supplied by stirring.

The rate of heat exchanged with the heat transfer fluid is calculated taking into account all the thermal resistances [16]: internal and film external resistances and reactor wall resistance.

3.2.1 Convective flux through the internal film resistance

$$\phi_{0\mathrm{w}} = h_{0\mathrm{w}} S_{\mathrm{w}} (T_{\mathrm{m}} - T_{0\mathrm{w}}) \tag{18}$$

The internal heat transfer coefficient, $h_{0\mathrm{w}}$, may be expressed as a function of operating conditions and fluid properties. It is deduced using dimensional analysis, from $\mathrm{Nu} = f(\mathrm{Re}, \mathrm{Pr}, \mathrm{Vi})$, and can be represented as a function of the stirring speed, N_{a}, by the following equation [17]

$$h_{0\mathrm{w}} = \alpha_0 N_{\mathrm{a}}^{\theta_{20}} \tag{19}$$

where α_0 is defined as a function of the mixture properties as

$$\alpha_0 = \theta_{10} \frac{\lambda_{\mathrm{m}}}{D_{\mathrm{R}}} \mathrm{Pr}^{\theta_{30}} \mathrm{Vi}^{\theta_{40}} \left(\frac{D_{\mathrm{a}}^2 \rho_{\mathrm{m}}}{\eta_{\mathrm{m}}} \right)^{\theta_{20}} \tag{20}$$

and where θ_{10}, θ_{20}, θ_{30}, θ_{40} are constants for each agitator, see Section 4.

The wetted surface is calculated as a function of the reaction mixture volume and the effect of stirring (vortex) [18]

$$S_{\mathrm{w}} = S_{\mathrm{B}} + \frac{2(V_{\mathrm{m}} - V_{\mathrm{B}})}{R_0} + \Delta S_{\mathrm{v}} \tag{21}$$

where S_{B} is the bottom surface, see Appendix 1, and ΔS_{V} is the surface increase due to the vortex.

3.2.2. Conductive radial flux through the reactor wall

The conductive radial flux from the reactor through the wall to the jacket is modelled with the following equations

— part wetted by the reaction mass

$$\phi_{w1} = \frac{2S_W \lambda_W}{e_w}(T_{0w} - T_{w1}) \tag{22}$$

$$\phi_{w2} = \frac{2S_w \lambda_w}{e_w}(T_{w1} - T_{1w}) \tag{23}$$

— dry part of the reactor wall

$$\phi_{w6} = \frac{2S_d \lambda_w}{e_w}(T_{0d} - T_{w2}) \tag{24}$$

$$\phi_{w7} = \frac{2S_d \lambda_w}{e_w}(T_{w2} - T_{1d}) \tag{25}$$

where e_w is the wall thickness, λ_w is the thermal conductivity of the wall and S_d is the exchange surface not wetted by the mixture, i.e. $S_T - S_w$, see Appendix 1.

3.2.3. Conductive axial flux through the reactor wall

$$\phi_{w3} = \frac{4S_x \lambda_w}{H_m}(T_{w1} - T_{1w}) \tag{26}$$

$$\phi_{w4} = \frac{2S_x \lambda_w}{H_m}(T_{w1} - T_{w2}) \tag{27}$$

$$\phi_{w5} = \frac{4S_x \lambda_w}{H_m}(T_{1w} - T_{1d}) \tag{28}$$

where

$$S_x = \pi(R_1^2 - R_0^2) \tag{29}$$

$$H_m = H_T - \frac{V_m}{\pi R_0^2} \tag{30}$$

The conductive axial flux, due to the low thermal conductivity of glass, has little influence in the energy balances.

3.2.4. Convective fluxes through the external film resistance

$$\phi_{1W} = h_1 S_w (T_{1w} - T_e)\Psi_1 \tag{31}$$

$$\phi_{1d} = h_1 S_d (T_{1d} - T_e)\Psi_2 \tag{32}$$

Replacing the relevant dimensionless numbers in the Nusselt equation [19], the external heat transfer coefficient, h_1, may be expressed as a function of the heat transfer fluid flow, Q_e, as

$$h_1 = \alpha_1 Q_e^{\theta_{21}} \tag{33}$$

where α_1 is defined as a function of the heat transfer fluid properties and jacket characteristics

$$\alpha_1 = \theta_{11} \frac{\lambda_e}{D_t} \mathrm{Pr}^{\theta_{31}} \mathrm{Vi}^{\theta_{41}} \left(\frac{\rho_e D_t}{S_t \eta_e} \right)^{\theta_{21}} \tag{34}$$

and $\theta_{11}, \theta_{21}, \theta_{31}, \theta_{41}$ are constants for each reactor and fluid-dynamic regime. Ψ_1 and Ψ_2 are correction factors to take into account the change in the heat transfer fluid temperature through the jacket

$$\Psi_1 = \left[\frac{1 - \exp\left(\frac{-h_1 S_w}{Q_e C_{pe}} \right)}{\frac{h_1 S_w}{Q_e C_{pe}}} \right] \tag{35}$$

$$\Psi_2 = \left[\frac{1 - \exp\left(\frac{-h_1 S_d}{Q_e C_{pe}} \right)}{\frac{h_1 S_d}{Q_e C_{pe}}} \right] \tag{36}$$

3.2.5. Thermal capacity of the wall

The thermal capacity of the reactor wall is divided into the part wetted by the reactant mass and the part that is maintained dry inside the reactor

$$\Gamma_{w_w} = \Gamma_w x_w \tag{37}$$

$$\Gamma_{w_d} = \Gamma_w - \Gamma_{w_w} \tag{38}$$

where x_w is the wetted surface fraction, $x_w = S_w/S_T$.

3.2.6. Heating/cooling by mass addition

During a semibatch process, frequently the added mass is not at the same temperature as the reactor, contributing to cooling or heating of the reactant mass. This enthalpy difference must then be taken into account in the energy balance

$$\phi_E = - \sum_{j \in A_L}^{N_L} F_{E_j} \int_{T_m}^{T_{E_j}} C_{p_j} \mathrm{d}T \tag{39}$$

where F_{E_j} is the molar input flow of j

$$F_{E_j} = \sum_{j \in A_L}^{N_L} Q_k C_{E_j} \; ; k = 1, .., N_E \tag{40}$$

where Q_k is the mass flow of the k input stream and C_{E_j} is the molality of j.

3.2.7. Heat losses

The importance of heat losses increases with the temperature difference between the system and the surroundings, also depending on how isolated the system is.

$$\phi_1 = US_1 (T_a - T_m) \tag{41}$$

where US_1 is the effective heat transfer coefficient for losses through the top of the reactor and T_a is the ambient temperature

3.2.8. Power supplied by stirring

Using dimensional analysis, it is possible to obtain an empirical law for the power introduced by the stirrer [17]

$$\mathrm{Po} = f(\mathrm{Re}, \mathrm{Fr}, S_1, S_2, \ldots S_n) \tag{42}$$

For agitated vessels, the dimensionless numbers can be defined as

$$\mathrm{Po} = \frac{\phi_a}{\rho_m N_a^3 D_a^5} \tag{43}$$

$$\mathrm{Re} = \frac{\rho_m N_a D_a^2}{\eta_m} \tag{44}$$

$$\mathrm{Fr} = \frac{N_a^2 D_a}{g} \tag{45}$$

$S_1, S_2, \ldots, S_n$ are shape factors, defined as the ratio between different characteristic geometric measures of the reactor related to the position of the stirrer,its diameter, the number of blades, etc.

From geometric similarity, Eq. (42) is reduced to

$$\mathrm{Po} = K_2 \mathrm{Re}^{K_3} \mathrm{Fr}^{K_4} \tag{46}$$

where K_2 is an overall dimensionless shape factor, and K_3 and K_4 are constants. Replacing the relevant terms of Eqs. (43)–(45) in Eq. (46), it is possible to obtain different situations for Newtonian fluids [20]: at low impeller Reynolds numbers, $\mathrm{Re} < 15$, the flow is laminar around the impeller and stagnant away from it; at higher Reynolds number, $\mathrm{Re} > 15$, discharge flow develops. This latter region is mostly laminar and extends up to $\mathrm{Re} \approx 200$ for turbine impellers. Beyond this point, the transition region begins with the flow becoming turbulent around the impeller, while further away the flow is still laminar. The transition region for impellers extends up to $\mathrm{R} \approx 10^4$. Thus, the average power input in an agitated vessel operating in the laminar region is given by

$$\phi_a = \alpha' \eta_m N_a^2 D_a^3 \tag{47}$$

In the transition range flow, the average power input in the vessel over short ranges is given by

$$\phi_a = \alpha'' \rho_m N_a^3 D_a^5 \left(\frac{\rho_m N_a D_a^2}{\eta_m} \right)^n \tag{48}$$

where α' and α'' can be considered constants, see Section 4.3, and n is the slope of the plot of the log of the power number versus of Re. With increasing Re, n increases continuously from -1 ($Re \approx 15$) to 0.16 ($Re \approx 300$) and then decreases, approaching 0 ($Re \approx 11000$).

3.2.9. Modification of the heat transfer area due to stirring (vortex)

The heat transfer area is the surface wetted by the reaction mixture and can be calculated as a function of the reaction mixture volume and the effect of stirring (vortex) using Eq. (21). To take into account the influence of the stirrer speed on the wetted surface due to the vortex produced by the agitator, the following correlation relating the increase in height of the exchange heat transfer area with the reactor radius and the stirrer speed was found in the literature [18]

$$H_v = \frac{N_a^2 R_0^2}{2g} \tag{49}$$

where H_v is the increase in height due to stirring. Hence

$$\Delta S_v = 2\pi R_0 H_v \tag{50}$$

This correlation is only valid for Newtonian fluids with no vertical or radial velocity. Experimental results have shown that this increase in the heat exchange area is dependent on liquid volume, the type of agitator, and the fluid physical properties. To correct the errors in Eq. (49), the value of n_a was multiplied by a factor, f, which depends empirically on all the characteristics mentioned above. Hence, Eq. (50) can be written, for a specified reactor and geometry, as

$$\Delta S_v = K_1 f N_a^2 \tag{51}$$

where K_1 is a constant that depends on the geometry of the reactor and f is a correction factor for non-idealities.

According to Uhl and Gray [17], the factor must be correlated with the discharge rate which depends on the power number given by Eq. (46). Substituting f by this term

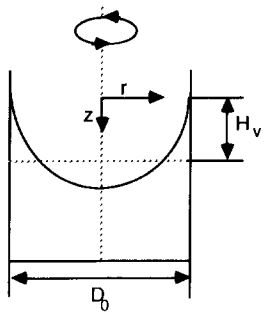

Fig. 3. Modification to the exchange surface due to stirring.

and rearranging Eq. (51) the following relationship is obtained

$$\Delta S_v = C_1 \mathrm{Re}^{C_2} \mathrm{Fr}^{C_3} N_a^2 g(V_m) \tag{52}$$

where $g(V_m)$ is a function that depends on the reaction mass volume. Intuitively, this function has to follow an exponential inverse behaviour, which means with less volume the increase in height must be bigger than with more volume present in the reactor. The correlation that better fitted the experimental data is

$$g(V_m) = \left(\frac{V_T - V_m}{V_T}\right)^{C_4} \tag{53}$$

where C_1, C_2, C_3 and C_4 are constants that were calculated experimentally for different fluids and agitators, modifying the liquid volume, the temperature and the stirrer speed, see Section 4.

3.2.10. Heat accumulation within the reactor

This term is calculated as the product of the molar hold-up with the specific heat of the component in the reactor, including the thermal capacity of the devices wetted by the mixture

$$\Gamma_m = \sum_{j \in A_L}^{N_L} n_{m_j} C_{p_{L_j}} + \Gamma_b \tag{54}$$

where Γ_b is the thermal capacity of the devices wetted, see Appendix 1.

4. Characterisation of the effective heat transfer coefficient and secondary heat effects

The most usual method to control temperature in batch reactors is by removing the heat generated by exothermic reactions during a process through a cooled heat transfer fluid that circulates in a jacket, see Fig. 4. The heat flow is proportional to the driving force (temperature difference between the reactor, T_m, and the jacket, T_e

$$\phi_0 = U \cdot S (T_m - T_e) \Psi \tag{55}$$

where the proportional factor $U.S$, called the effective heat transfer coefficient, depends

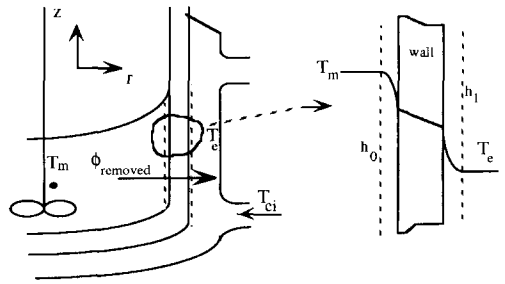

Fig. 4. Heat transfer from a chemical reactor to an external jacket.

on the fluid properties, operating conditions and the geometry of the system. Ψ is a correction factor to take into account the change in the heat transfer fluid temperature between the inlet and the outlet of the jacket.

Knowledge of $U.S$ is of great importance for the design of batch reactors. Different experimental and empirical methods have been proposed to evaluate the effective heat transfer coefficients for which heat flow calorimetry has demonstrated to be a useful technique [21] and it is widely used. The method consists of introducing a known thermal power in the reaction mass, ϕ_i, by means of an electrical resistance and comparing the area under the curve of a plot of $(T_m - T_e)\Psi$ against time over a period of calibration [28], while using the control system to keep the reactor temperature constant

$$U \cdot S = \frac{\phi_i}{(T_m - T_e)\Psi} \tag{56}$$

4.1. Experimental description

In order to validate experimentally the model for the calculation of $U \cdot S$, a set of experiments with five different fluids, isopropanol, tetrachloromethane, ethylene glycol, water and toluene, was carried out in the RC1. The type of stirrers used were anchor and two turbines for L/L and G/L mixtures, with a speed range of 50–250 rpm for the anchor, and of 200–800 rpm for the turbines. The temperature and volume ranges were 273–323 K and 0.7–1.8 l respectively. The experimental results for 1 l of tetrachloromethane are shown in Table 1 as an example. The influence of the exchange surface on $U.S$ was investigated for the cases of water and toluene, carrying out a series of evaluations, periodically adding a certain amount of the liquid and using a different type of stirrer. Table 2 shows the experimental results for water.

The values, obtained in the experiments described previously, were employed to evaluate the participation of resistances involved in the overall heat transfer coefficient, and to adjust the expression for the wetted surface.

The parameters for the internal heat transfer coefficient, see Table 3, were found in the literature [21]. The θ_{12} and θ_{21} of the external heat transfer coefficient, h_1, and C_1, C_2, C_3 and C_4, Eqs. (52) and (53), for each stirrer were adjusted using a multivariable non-linear regression method [22]. These values are shown in Tables 4 and 5. The results form a comparison between the experimental evaluation and the predicted values are: maximum error 10.3%, average error 2.3%, standard deviation 2.8%. Fig. 5 shows experimental and calculated results for toluene and water respectively.

4.2. Power introduced by stirring into the reaction mass

Different experiments were performed with water in order to determine if the data obtained were consistent with literature correlations. The experiments consisted of following the increase in temperature as a function of time over a period of one day under adiabatic conditions. For the two types of agitators tested (anchor and turbine), the agreement was satisfactory and consequently the data from the literature [17, 21] were employed to calculate the power introduced by stirring the reaction medium.

Table 1
$U \cdot S$ ($W K^{-1}$) for 1 l of tetrachloromethane with the anchor, turbine G/L and turbine L/L stirrers as a function of temperature and stirrer speed

T_m/°C	Anchor stirrer/rpm				
	50	100	150	200	250
0.0	4.158	4.947	5.573	6.132	6.737
15.0	4.328	5.116	5.781	6.337	6.918
25.0	4.370	5.260	5.829	6.421	7.038
35.0	4.483	5.358	6.051	6.569	7.149
50.0	4.643	5.634	6.384	6.865	7.416
T_m/°C	Turbine G/L stirrer/rpm				
	200	300	400	500	600
0.0	4.799	5.190	5.537	5.959	6.419
15.0	4.950	5.402	5.778	6.256	6.657
25.0	5.080	5.524	5.892	6.379	6.803
35.0	5.213	5.642	6.064	6.542	6.993
50.0	5.381	5.957	6.432	6.977	7.357
T_m/°C	Turbine L/L stirrer/rpm				
	200	300	400	500	600
0.0	4.849	5.244	5.583	6.026	6.516
15.0	5.041	5.406	5.790	6.257	6.703
25.0	5.141	5.522	5.839	6.405	6.862
35.0	5.235	5.665	6.064	6.639	7.031
50.0	5.436	5.947	6.464	7.096	7.499

4.3. Heat losses

The following expression [23] was used in order to take into account the heat losses, mainly, from the reactor cover to the surroundings

$$\phi_1 = (8.1 \times 10^{-3} T_m - 2.348)(T_a - T_m) \tag{57}$$

5. Modelling and characterisation of the heating/cooling circuits and controllers

5.1. Introduction

The thermostat basically consists of two different loops where silicone oil, used as a heat transfer fluid, circulates at high speed. The first loop contains electrical heater, that can give power up to 2000 W and is connected to the jacket in which the silicone oil

Table 2
Variation of $U \cdot S$ (W K^{-1}) for water as a function of the volume in the reactor for the anchor stirrer at 250 rpm and for the turbine G/L and L/L at 500 rpm and 308 K

Mass of water/kg	$U \cdot S$ anchor	$U \cdot S$ turbine G/L	$U \cdot S$ turbine L/L
0.717	6.769	6.071	5.835
0.767	6.901	6.077	5.946
0.817	7.153	6.289	6.102
0.867	7.378	6.387	6.264
0.917	7.492	6.571	6.409
0.967	7.620	6.696	6.614
1.017	7.699	6.806	6.705
1.067	7.879	6.949	6.860
1.117	7.919	7.187	7.082
1.167	8.128	7.325	7.217
1.217	8.195	7.469	7.338
1.267	8.340	7.587	7.544
1.317	8.451	7.793	7.669
1.367	8.556	7.923	
1.417	8.568	7.969	7.965
1.467	8.666	8.163	8.130
1.517	8.736	8.414	8.232
1.567	8.845	8.512	8.393
1.617	8.898	8.648	8.556
1.667	–	8.777	8.661
1.717	–	8.927	–
1.767	–	8.959	–
1.817	9.180	9.073	8.953

Table 3
Coefficients for the exponents of h_0, Eqs. (26) and (27)

Coefficients	Anchor	Turbine
θ_{10}	0.29	0.42
θ_{20}	0.678	0.694
θ_{30}	1/3	1/3
θ_{40}	0.14	0.14

Table 4
Coefficients for the exponents of h_1, Eqs. (40) and (41)

Coefficients	Annular jacket, no baffles
θ_{11}	1.14
θ_{21}	0.29
θ_{31}	1/3
θ_{41}	0.14

Table 5
Values of the constants of Eqs. (52) and (53) for the reaction calorimeter

Constant	Anchor	G/L Turbine	L/L Turbine
C_1	1.251×10^{-3}	0.917×10^{-5}	1.36×10^{-5}
C_2	−0.0145	0.325	0.284
C_3	−0.309	−0.395	−0.486
C_4	1.11	1.66	1.80

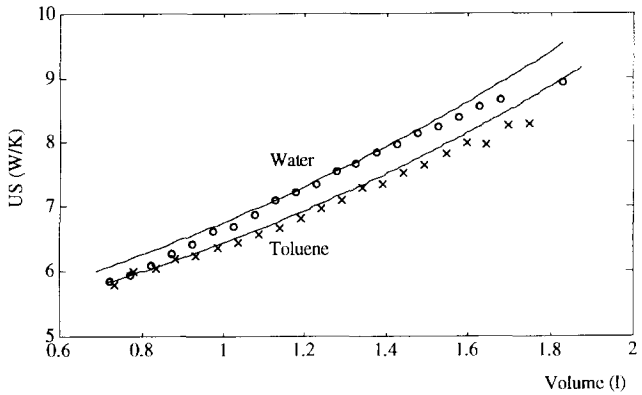

Fig. 5. Experimental and calculated effective heat transfer coefficient for pure water and toluene. Periodical additions were carried out followed by evaluation of US. $T_m = 308$ K, and $n_a = 8.33\,s^{-1}$.

is pumped (approx. 3 l capacity). The second loop is the cooling circulation system, with a larger capacity (approx. 5 l), connected to the heating loop by a control valve and containing a coil heat exchanger attached to an external cold source, see Fig. 6. To follow a programme, the temperature of the heat transfer fluid in the jacket is adjusted by manipulating the electrical heater and/or the control valve.

The cooling flow, Q_c, and the electrical heating power, ϕ_h, are manipulated by the controller according to a cascade control scheme described in Fig. 7.

The controller of the outer loop (CI) corrects deviations of the reactor temperature from the set value T_{sp}, following a P (Proportional) criterion using a P_1 value defined beforehand by the user to calculate the set-point of jacket temperature

$$T_{esp} = T_{sp} + P_1(T_{sp} - T_m) \tag{58}$$

providing the set value for the heat transfer fluid temperature, T_{esp}, which is adjusted by the inner loop controller (C2) by means of a self-adaptive PI (Proportional-Integral) criterion. Controller C2 uses a model-based algorithm which carries out an energy balance in the heated loop at each sampling time, calculating the power necessary to

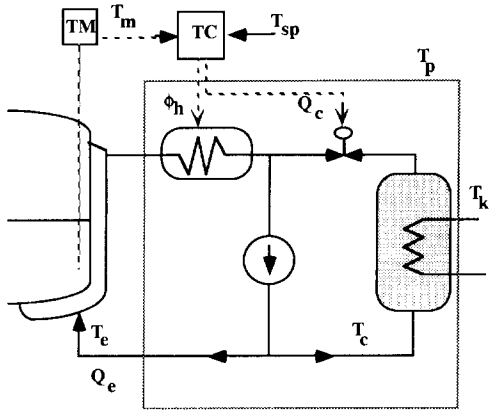

Fig. 6. Thermostat of the reaction calorimeter.

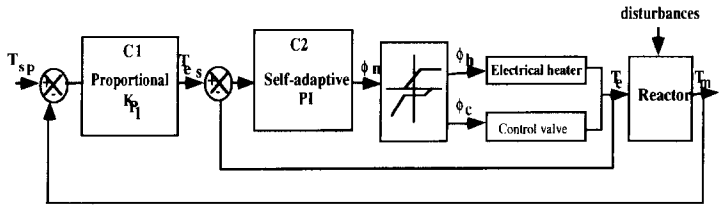

Fig. 7. Temperature control scheme.

reach or maintain the required temperature

$$\phi_n = P_2(T_{e_{sp}} - T_e) + I_2 \int (T_{e_{sp}} - T_e)dt - \phi_{pumps} - \phi_{losses} \tag{59}$$

where, respectively, ϕ_{pumps} and ϕ_{losses} take into account the power introduced due to friction by the recirculating pumps, and the heat losses of the thermostat to the surroundings, see Table 7.

The controller distributes this power by acting either on the electrical resistance or on the control valve according to an empirical criterion [24] which decomposes the needed power, ϕ_n, into the two different components, i.e. heating power, ϕ_h, and cooling power, ϕ_c, see Fig. 8.

5.2. *Modelling the heating/cooling circuits*

In order to reproduce the behaviour of the RC1 under any operating mode, the simulator has to predict the evolution of the heat transfer fluid temperature and consequently a model of the thermostat functioning was developed. According to the characteristics of the heating/cooling circuits, and after having tested different types of

Table 7
Characteristic values of the controllers [23]

Parameter	Value
P_1	3–12
P_2	700
I_2	4.5
q_{pumps}/W	120.0
q_{losses}/W	$6.6(298.0 - T_e)$

modelling, it was found that a model consisting of three thermally homogeneous subsystems described adequately the behaviour of these circuits: the heated and cooled loops with temperatures T_e and T_c, respectively, and the container of the heat loop with uniform temperature T_p. Energy balances in the three subsystems permitted the time-profile of temperatures T_e, T_c and T_p to be mathematically modelled, and the control algorithm to be applied

$$\frac{dT_e}{dt} = \frac{1}{\Gamma_e}[\phi_0 + Q_c\rho_e C_{p_e}(T_c - T_e) + \phi_h + \phi_{p_e}] + \frac{(T_p - T_e)}{\tau_{e_1}} \tag{60}$$

$$\frac{dT_c}{dt} = \frac{1}{\Gamma_c}[-Q_c\rho_e C_{p_c}(T_c - T_e) - US_c\Delta T_{ln} + \phi_{p_c} + US_{lc}(T_a - T_c)] \tag{61}$$

$$\frac{dT_P}{dt} = \frac{T_a - T_P}{\tau_P} + \frac{T_e - T_P}{\tau_{e_2}} \tag{62}$$

where Γ_e, Γ_c are the overall thermal capacities (oil + inserts) of the heating and cooling loops; q_0 is the heat exchanged with the reactor wall $= \phi_{0w} + \phi_{0d}$; ϕ_{pe}, ϕ_{pc} are the thermal fluxes due to the recirculating pumps; US_c is the effective heat transfer coefficient between the cooling loop and the external cold source, i.e. the cryostat; ΔT_{ln}

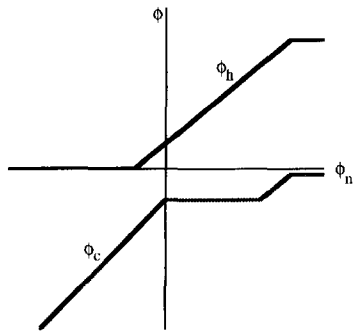

Fig. 8. Heating/cooling split.

is the logarithmic average temperature of heat exchange between the cooling loop and the external cold source; τ_{e1} and τ_{e2} are time constants of heat exchange between the heated loop and its container; τ_p is the time constant of heat losses of the container of the heated loop; and US_{lc} is the overall heat loss coefficient in the cooled circuit.

5.3. *Heating/cooling circuit characteristics*

Different aspects have been studied in order to characterise completely the different variables and parameters of the model of the heating/cooling circuit formulated above. These are:

(i) Power introduced by the centrifugal pumps (ϕ_{pe} and ϕ_{pc}) [25]

The power introduced to the heat transfer fluid from the centrifugal pumps due to friction effects, can be described as a function of the viscosity by the following equations

$$\phi_{pe} = 59.14 + 0.86 \times 10^3 \eta_e \tag{63}$$

$$\phi_{pc} = 24.63 + 0.37 \times 10^3 \eta_c \tag{64}$$

where η_e and η_c are the viscosities of the heating and cooling circuits, respectively, see Appendix 1.

(ii) Flow of the heat transfer fluid (Q_e)

The hydraulic characteristics of the heating/cooling circuit were experimentally determined [26]. A hysteresis behaviour was observed: for a given temperature, the flow characteristics were different for the cases where the steady state was reached by increasing or decreasing the temperature of the heat transfer fluid.

For simulation purposes, the following correlation, see Fig. 9, was used in the evaluation of the heat transfer coefficients

$$Q_e = -7.565 \times 10^{-4} + 4.631 \times 10^{-6} T_e - 4.238 \times 10^{-9} T_e^2 \tag{65}$$

(iii) Steady state experiments

Experiments to determine some characteristic parameters of the heating/cooling circuits, were performed in steady state conditions, i.e.

$$\frac{dT_e}{dt} = 0, \quad \frac{dT_c}{dt} = 0, \quad \text{and} \quad \frac{dT_p}{dt} = 0 \tag{66}$$

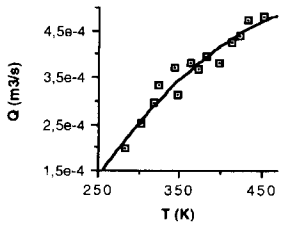

Fig. 9. Volumetric flow as a function of heat transfer fluid temperature [24].

The first set of experiments was carried out on introducing a constant power by means of the electrical heater, maintaining a constant external cryostat temperature, and forcing the control valve to be fully open by a fictitious set-point value. For each experiment, the system was brought to a steady state after a certain period of time. The experimental values found are listed in Table 8.

Another set of experiments was carried out in the same way, but forcing the control valve to be fully closed and without introducing any power. In this case, the different steady states were reached by changing the temperature of the external cold source (T_K). For each experiment the system was brought to a steady state after a certain period of time. The experimental values found are listed in Table 9.

Table 8
Steady state values with fully open control valve

ϕ_h/W	T_K/°C	T_a/°C	T_c/°C	T_c/°C	ΔT_K
1796.0	11.9	24.5	66.15	24.0	3.590
1973.0	0.0	24.7	59.30	14.05	4.320
1974.0	−7.8	24.5	52.50	6.9	4.835
1327.0	−8.0	24.5	32.50	2.8	3.420
980.4	−8.2	24.0	23.40	0.47	2.690
700.1	−8.2	24.0	15.50	−1.40	2.020
412.7	−8.3	24.0	8.16	−3.25	1.430
1976.0	−15.5	24.5	45.50	0.10	5.760
1642.0	−15.5	25.5	35.90	−2.00	4.580
1329.0	−15.6	24.5	26.32	−4.10	4.230
988.6	−15.7	24.5	16.90	−6.40	3.390
698.1	−15.8	24.0	9.20	−8.30	2.640
418.7	−15.81	24.5	1.56	−10.30	1.910
207.7	−15.85	24.5	−4.00	−11.75	1.310
54.4	−15.9	24.2	−7.94	−12.90	0.860
693.6	−19.8	22.0	5.58	−12.10	2.980
412.7	−19.9	21.0	−2.12	−14.10	2.140
204.4	−20.0	21.0	−7.61	−15.60	1.550
66.5	−20.0	21.0	−11.20	−16.60	1.160
16.8	−20.0	21.0	−12.58	−17.00	0.961
0.0	−20.0	21.0	−12.97	−17.10	0.940
700.0	−23.7	23.5	2.45	−15.45	3.630
417.6	−23.85	23.5	0.31	−17.80	2.670
207.7	−23.9	23.5		−19.50	1.850
1266.0	10.0	25.1	47.70	19.00	
1266.0	2.0	25.1	40.13	11.65	
1266.0	−6.0	25.2	32.70	4.20	
1266.0	−15.0	25.0	25.25	−3.70	
1266.0	−22.0	25.0	19.60	−9.50	
1266.0	−30.0	25.0	18.80	−10.10	
0.0	19.6	21.3	23.33	21.29	
0.0	17.7	21.5	21.54	19.39	

Table 9
Steady state values with fully close control valve

h/W	T_K/°C	T_a/°C	T_e/°C	T_c/°C
0.0	0.0	19.14	38.27	1.302
0.0	−10.0	19.23	34.79	−8.47
0.0	−20.0	18.88	30.81	−17.97
0.0	−30.0	18.75	27.02	−27.20
0.0	−30.0	10.42	24.18	−27.20

Inserting the steady state condition, Eq. (66), into Eqs (60)–(62), the following equations are obtained

$$Q_c \rho_e C_{p_e}(T_c - T_e) + \phi_h + \phi_{p_e} + \frac{\Gamma_e (T_p - T_e)}{\tau_{e_1}} = 0 \tag{67}$$

$$-Q_c \rho_e C_{p_e}(T_c - T_e) - US_c \Delta T_{ln} + \phi_{p_c} + US_{1c}(T_a - T_c) = 0 \tag{68}$$

$$\frac{T_a - T_P}{\tau_P} + \frac{T_e - T_P}{\tau_{e_2}} = 0 \tag{69}$$

Using Eq. (69) to obtain an expression for T_P

$$T_p = \frac{\tau_{e_2} T_a + \tau_p T_e}{\tau_{e_2} + \tau_p} \tag{70}$$

Replacing this equation in Eq. (67) and rearranging,

$$T_e = \frac{\phi_h + \phi_{p_e} + K_1 T_a}{Q_c \rho_e C_{p_e} + K_1} + \frac{Q_c \rho_e C_{p_e}}{Q_c \rho_e C_{p_e} + K_1} T_c \tag{71}$$

where K_1 is defined as,

$$K_1 = \frac{\tau_{e_2} \Gamma_e}{\tau_{e_1}(\tau_p + \tau_{e_2})} \tag{72}$$

As a first approximation, this term was considered a constant related to the properties of the system (masses and heat capacities) and the heat losses of the heating loop.
(iv) Maximum and minimum flow through the control valve ($Q_{c_{max}}$ and $Q_{c_{min}}$) and K_1 In order to evaluate the maximum flow through the control valve, eq. (71) was applied with the experimental points of Table 8. Representing T_e as a function of T_c, assuming that $Q_{c_{max}}$ and K_1 are constants and the heat transfer fluid properties (C_{pe}, ρ_e) do not change appreciably in the temperature range considered, the experimental values should give different straight lines for each constant power input (ϕ_h) at the same ambient temperature. Fig. 10 seems to confirm such a hypothesis.

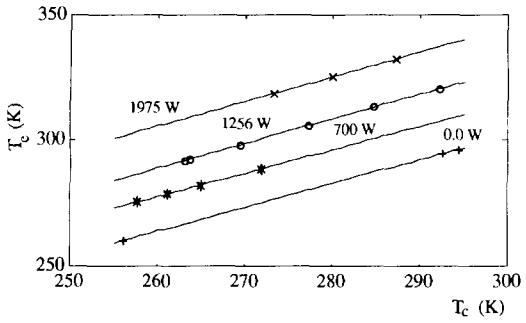

Fig. 10. T_e versus T_c for different power inputs with opened control valve.

The values obtained for the different straight lines are

$$T_{e\,(1975.0)} = 48.52 + 0.989\,T_c \tag{73}$$

$$T_{e\,(1266.0)} = 33.10 + 0.984\,T_c \tag{74}$$

$$T_{e\,(700.0)} = 36.13 + 0.929\,T_c \tag{75}$$

$$T_{e\,(415.0)} = 25.99 + 0.946\,T_c \tag{76}$$

$$T_{e\,(0.0)} = 18.05 + 0.946\,T_c \tag{77}$$

From these series of experiments, replacing the values of eqs. (73)–(77) in Eq. (71), the value calculated for $Q_{c_{max}}$ was
$Q_{c_{max}} = (3.09 \pm 0.42)\,10^{-5}\ m^3\,s^{-1}$
The same procedure was followed in order to calculate the minimum flow through the control valve using the experimental results of Table 9. Representing T_e as a function of T_c, see Fig. 11, the straight line was fitted to

$$T_e = 202.64 + 0.397\,T_c \tag{78}$$

and replacing the values of Eq. (78) in Eq. (71) the value obtained for $Q_{c_{min}}$ was$Q_{c_{max}} = (7.34 \pm 0.04) \times 10^{-7}\,m^3\,s^{-1}$

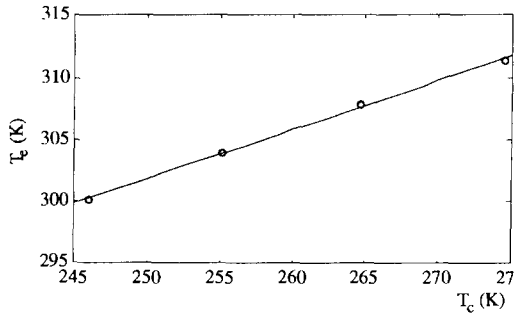

Fig. 11. T_e versus T_c with control valve closed.

The corresponding values of K_1 were also determined following the same procedure $K_1 = 2.2 \pm 1.6$

(v) Cooling provided by the external source and US_{1c}.

The heat exchanged by the cooling loop through the external cold source can be expressed as

$$\phi_{\text{exchanged}} = US_c \Delta T_{ln} \tag{79}$$

where US_c is the overall heat transfer coefficient for the internal coil of the cooling circuit multiplied by the exchange area, and ΔT_{ln} is the logarithmic average temperature of the heat exchange between the cooling loop and the external cold source. ΔT_{ln} can be calculated using the following expression

$$\Delta T_{ln} = \frac{T_{K_o} - T_{K_i}}{\ln\left(\frac{T_c - T_{K_i}}{T_c - T_{K_o}}\right)} \tag{80}$$

Hence, T_{K_o} is the only unknown. From a heat balance in the coil of the cooling loop, and neglecting the accumulation term

$$T_{K_o} = T_c + (T_{K_i} - T_c)\exp\left(\frac{-US_c}{Q_K \rho_K C_{pK}}\right) \tag{81}$$

The exponential term depends on the cryostat properties and characteristics of the cooling loop. In the normal operation mode, the cryostat conditions should be more or less constant and therefore the exponential term can be assumed constant as first approximation. Then Eq. (81) reduces to

$$T_{K_o} = T_{K_i} E_1 + T_c(1 - E_1) \tag{82}$$

with

$$E_1 = \exp\left(\frac{-US_c}{Q_K \rho_K C_{p_K}}\right) \tag{83}$$

Hence, rearranging eq. (83) it is possible to find

$$E_1 = \frac{T_{K_o} - T_c}{T_{K_i} - T_c} \tag{84}$$

This assumption was validated experimentally in the experiments at steady state. In these experiments ΔT_K was measured by means of a precise device, a Hewlett Packard mod. 2804A. The experimental data found are listed in Table 10.

Taking the average, $E_1 = 0.655$, then eq. (82) becomes

$$T_{K_o} = 0.655\ T_{K_i} + 0.345 T_c \tag{85}$$

By manipulating Eq. (68), it is possible to obtain the following expression for the evaluation of US_c

$$T_e = \frac{US_c \Delta T_{ln} - \phi_{pc} - US_{1c} T_a}{Q \rho_e C_{pe}} + \frac{Q_c \rho_e C_{pe} + US_{1c}}{Q_c \rho_e C_{pe}} T_c \tag{86}$$

Table 10
Experiments to determine the cooling provide by the external source

T_c/°C	T_{K_i}/°C	T_{K_o}/°C	E_1
24.0	11.90	15.49	0.703
14.1	0.00	4.32	0.694
6.9	−7.80	−2.97	0.671
2.8	−8.00	−4.58	0.683
0.5	−8.20	−5.51	0.691
−1.4	−8.20	−6.18	0.703
−3.3	−8.30	−6.87	0.714
0.1	−15.50	−9.74	0.631
−2.0	−15.50	−10.92	0.661
−4.1	−15.60	−11.37	0.632
−6.4	−15.70	−12.31	0.635
−8.3	−15.80	−13.16	0.648
−10.3	−15.81	−13.90	0.653
−11.8	−15.85	−14.54	0.677
−12.9	−15.90	−15.04	0.713
−12.1	−19.80	−16.82	0.613
−14.1	−19.90	−17.76	0.631
−15.6	−20.00	−18.45	0.648
−16.6	−20.00	−18.84	0.659
−17.0	−20.00	−19.04	0.680
−17.1	−20.00	−19.06	0.676
−15.5	−23.70	−20.07	0.557
−17.8	−23.85	−21.18	0.559
−19.5	−23.90	−22.05	0.580

The slope of the correlations for the experimental values (see Fig.10) suggests that the evaluation of US_{1c} from this data will be difficult since $Q_c \rho_e C_{pe} \gg US_{1c}$. This implies that in the second term of eq. (86), the factor that multiplies T_c is approximately . Using this simplification and rearranging, eq. (86) becomes

$$US_c \Delta T_{1n} - Q_c \rho_e C_{p_e}(T_e - T_c) - \phi_{p_c} - US_{1c} T_a = 0 \tag{87}$$

In order to evaluate the evolution of US_C as a function of the temperature of the external cryostat (T_K) and the internal cooling loop (T_c), the following assumption was made

$$US_c = A + BT_{cK} + CT_{cK}^2 \tag{88}$$

where T_{cK} is an average temperature defined as

$$T_{cK} = \frac{\left(\frac{T_{K_i} + T_{K_o}}{2}\right) + T_c}{2} \tag{89}$$

From regression analysis, the parameters of Eqs.(86) and (87) were obtained, see Table 11.

Table 11
Parameters for the calculation of US_c and Us_{1c}

A	-2.670×10^3
B	19.36
C	-3.262×10^{-2}
Us_{1c}/W K^{-1}	0.435

(vi) Experiments in dynamic conditions, thermal capacities and time constants (Γ_e, Γ_c, τ_P, τ_{e1}, τ_{e2})

A set of curves, see Fig .12, were generated by means of jumps in the temperature set values using the empty reaction calorimeter in order to characterize the thermal capacities and time constants of the different parts of the heating/cooling loop.

It is possible to obtain Eqs. (90) and (91) from the start of the heating period (maximum heating) and Eqs. (92) and (93) from the start of the cooling period (maximum cooling) part of the curves, with the following assumptions:

— Thermal equilibria at the beginning of the experiments, i.e. no heat accumulation on the wall of the main loop.

— Starting the heating: the system control closes the regulation valve completely ($Q_c = Q_{c_{min}}$) and the electrical heater introduces the maximum power ($\phi_h = 2000$ W).

— Starting the cooling: the system control opens the regulation valve completely ($Q_c = Q_{c_{max}}$) and the electrical heater is off ($\phi_h = 0$ W)

— $(T_p - T_e) \approx 0$

$$\Gamma_e\left(\frac{dT_e}{dt}\right)_{max} = Q_{c_{min}}\rho_e C_{p_e}(T_c - T_e) + 2000.0 + \phi_{p_e} \tag{90}$$

$$\Gamma_c\left(\frac{dT_c}{dt}\right)_{min} = Q_{c_{min}}\rho_e C_{\sigma^e}(T_c - T_e) - US_c\Delta T_{1n} + \phi_{p_c} + US_{1c}(T_a - T_c) \tag{91}$$

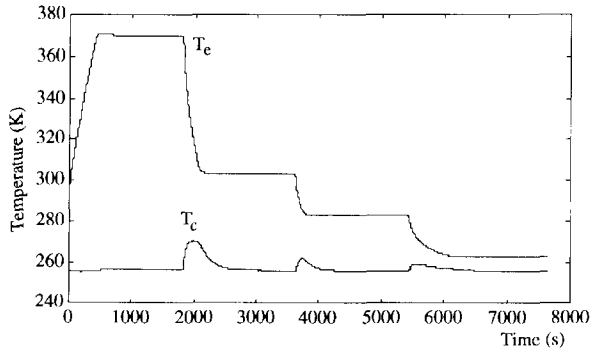

Fig. 12. Maximum heating and cooling rate in isoperibolic mode with empty reactor. T_{sp}: 293.2 → 370.2 → 283.2 → 263.2 K.

for the maximum heating period, and

$$\Gamma_e\left(\frac{dT_e}{dt}\right)_{min} = Q_{c_{max}}\rho_e C_{p_e}(T_c - T_e) + 0.00 + \phi_{p_e} \tag{92}$$

$$\Gamma_c\left(\frac{dT_c}{dt}\right)_{max} = -Q_{c_{max}}\rho_e C_{p_e}(T_c - T_e) - US_c\Delta T_{1n} + \phi_{p_c} + US_{1c}(T_a - T_c) \tag{93}$$

for the maximum cooling period.

Unfortunately, the derivative and, in particular, the search for its maximum and minimum is very sensitive to noise and the type of filtering and/or data treatment, but the following approximate values were obtained

$$\Gamma_e \approx 5.0 \times 10^3\,\mathrm{J\,K^{-1}}$$

$$\Gamma_c \approx 2.0 \times 10^4\,\mathrm{J\,K^{-1}}$$

The time constants τ_{e1}, τ_{e2}, and τ_P are difficult to evaluate from experiments due to the fact that T_P is not measured and probably not constant. However, orders of magnitude can be calculated with the data available (assuming a certain weight for the container of the heated loop made of stainless steel) and considering the following relationships

$$\tau_{e_1} = \frac{\Gamma_e}{US_P} \quad \tau_{e_2} = \frac{\Gamma_P}{US_P} \quad \text{and} \quad \tau_P = \frac{\Gamma_P}{US_a} \tag{94}$$

$$\tau_{e1} \approx 20.0\,\mathrm{s}$$

$$\tau_{e2} \approx 30.0\,\mathrm{s}$$

$$\tau_P \approx 2000.0\,\mathrm{s}$$

In order to fit the heating/cooling model to the experimental results, the set of curves generated in isoperibolic mode, i.e. constant jacket temperature, were used to obtain the remainder of the unknowns. After an optimisation procedure [22] the results obtained are listed in Table 12.

Using Eq. (72) with the values of Table 12, the value found for $K_1 \approx 1$ is consistent with the values calculated from steady-state experiments.

Table 12
Results of the optimisation procedure

Constants	value
Γ_e/J K^{-1}	3.59×10^3
Γ_c/J K^{-1}	1.7×10^4
τ_P/s	7747.0
τ_{e1}/s	18.07
τ_{e2}/s	38.82

6. Implementation of the numerical simulator

According to the objectives and the requirements, the simulator was developed in terms of independent modules as shown in Fig. 13. The physico-chemical properties of the substances dealt with, the stoichiometry and the thermo-kinetic parameters of reactions are introduced beforehand by the user. Concerning this aspect, full flexibility is permitted, e.g. any number of components and complex reaction schemes. This information, as well as the equipment characteristics of the reaction calorimeter, is managed and stored in the DATA LIBRARY block.

For a given case, the user introduces an operating procedure which is validated and interpreted by the algorithms of the INPUT block which by accessing the respective libraries, generate a matrix structure containing all the information necessary for the simulation and used by the SEQUENCE.

The SEQUENCER controls the simulation and sends the results to the OUTPUT block. This control consists of timing the simulation and updating the matrix structure by interacting with the MODEL GENERATOR and the SOLVER.

The MODEL GENERATOR constructs a set of algebraic-differential equations whose number depends on the specific case and administers any modification of the model during simulation. Mathematical models implemented in the simulator comprise a basic model considering a homogeneous mixture and ideal behaviour, and alternative models, which are collected cases of particular interest or systems for which the assumptions of the basic model are not valid.

The basic model consists of fundamental equations like heat and mass balances, and equilibrium relations, reproducing the behaviour of the state vector and of thermo-kinetic models representing all the thermal fluxes involved in the process. Special emphasis has been placed on the evaluation of physico-chemical and transport properties. Correlations obtained by dimensionless analysis are used in order to follow the influence of the main operating variables, such as stirrer speed, reactant feeding rate, temperature and flow of the heat transfer fluid.

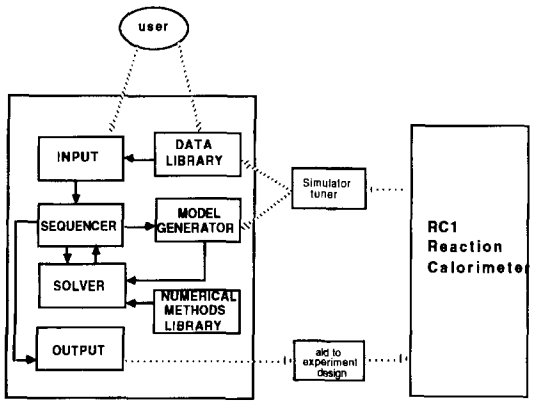

Fig. 13. Block diagram of the simulator and its interaction with the reaction calorimeter.

The simulator also includes models for the controllers of temperature, and reactant flows. Due to the complexity and fast response of the cooling/heating circuit and in order to reproduce the isothermal-controlled operating mode, it was necessary to model the dynamic behaviour of the heat transfer fluid.

The numerical resolution of the set of equations is done by the SOLVER block, which uses numerical tools available in the NUMERICAL METHODS LIBRARY.

The results presented by the OUTPUT block, in tabulated or graphic format, are the profiles of temperature, pressure, volume, composition and thermal fluxes as functions of time.

The whole code was implemented in FORTRAN-77 on a PC.

7. Model validation tests

A set of different experiments was carried out in order to examine the assumptions in the model and to compare the experimental and predicted dynamic behaviour. The first set consisted of heating/cooling the reactor by means of jumps in the temperature set values of the reaction calorimeter. In the second set, a very simple reaction, i.e. neutralisation, was chosen and several experiments modifying the operating conditions, such as temperature, concentrations, feeding rate, etc., were carried out.

7.1. Heating/cooling tests

With the reactor filled with 1.00 l of water, different heating and cooling experiments were carried out by the same procedure followed in Section 5.3. The aim of these tests was to compare the experimental behaviour of the reaction calorimeter with the behaviour predicted by the simulator for some step changes on the temperature set-point. The temperature of the cryostat was maintained constant and equal to -20°C.

Note that during the experiments some calibrations that were not simulated were carried out. The same types of experiments were performed, filling the reactor with 0.6 l of 2-butanol. In this case, the capacity for predicting the internal heat transfer coefficient as a function of the physical properties for a liquid that was not used in the *U.S* characterisation experiments was also evaluated.

As can be seen from Figs. 14 and 15, the simulator is able to predict correctly the dynamic behaviour of the reactor, jacket and cooling reservoir temperatures in a wide range (more than 100 K), even for a liquid that was previously not used during the characterization phase.

The next step during the validation of the simulator was to include a simple reaction carried out in semibatch to test the influence of the feeding and the thermo-kinetic data.

7.2. Neutralisation reaction

The neutralisation reaction between sodium hydroxide and hydrogen chloride is an example of an instaneous and irreversible chemical reaction, i.e. the power generated by the reaction medium is proportional to the speed of introduction of reactants

$$HCl_{aq} + NaOH_{aq} \rightarrow NaCl_{aq} + H_2O$$

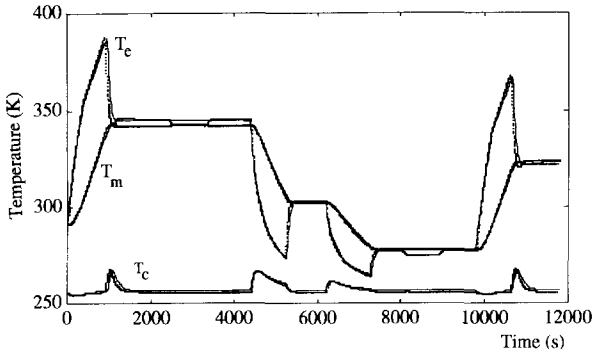

Fig. 14. Experimental (dotted lines) and simulated (continuous lines) behaviour of different steps with water. T_{sp}: 291.7 → 343.2 → 283.2 → 262.2 → 323.2 K.

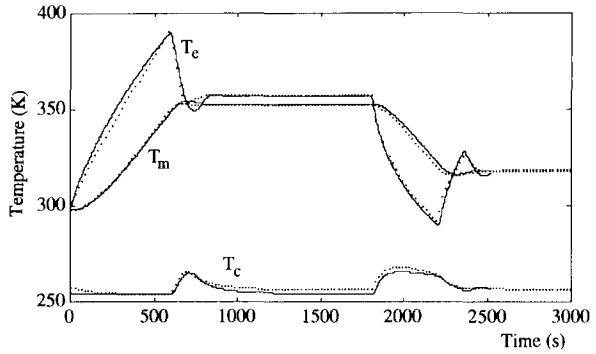

Fig. 15. Experimental (dotted lines) and simulated (continuous lines) of different steps with 2-butanol. T_{sp}: 298.2 → 353.2 → 318.2 K.

The heat of neutralisation at 25°C [27] is $-55.9\ \text{kJ mol}^{-1}$. Due to the reaction being instantaneous, the rate of reaction is defined as follows

$$r(t) = \frac{Q_{E_j} C_{E_j}}{V_m(t)} = \frac{F_{E_j}}{V_m(t)} \tag{95}$$

An aqueous solution of hydrogen chloride, approx. 2 M, was added to the reactor. When the reactor temperature was stabilised to the set-point temperature, the sodium hydroxide solution, approx. 2 M, was introduced.

Two defferent operating modes were carried out with the purpose of testing the dynamics of the simulator:

— In isoperibolic mode, T_e was maintained constant and a two additions of NaOH solution were performed at constant rate. As can be seen in Fig. 16, the agreement is

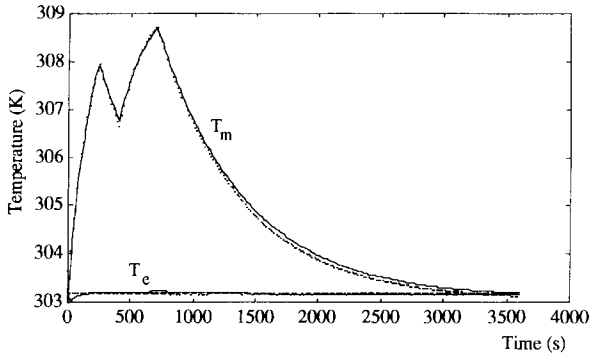

Fig. 16. Experimental (dotted lines) and simulated (continuous lines) behaviour during an isoperibolic experiment. Initial conditions: 1.3 mol HCl, 32.7 mol H_2O and T_e = constant = 303.2 K; anchor stirrer, 200 rpm. Two additions of NaOH solution at 1.3 gs^{-1} of dosing rate. First addition: 0.6 mol NaOH and 15.9 mol of H_2O. Second addition: 1.6 mol NaOH and 46.2 mol H_2O.

satisfactory during the heating and cooling periods. Under these conditions, the simulator does not solve the differential equations of the heating/cooling system, but maintains the jacket temperature constant, see T_e profile in Fig. 16.

— In the isothermic mode, the same type of procedure was followed but the temperature of the reactor T_m was kept at the specified set-point by the control system, and the proportional controller was set to 10 according to the Mettler RC1 operating instructions [28]. In these experiments the dynamic behaviour of the simulated heating/cooling circuits was also tested. As can be seen in Figs. 17–19, the agreement between experimental and simulated dynamic behaviour is satisfactory.

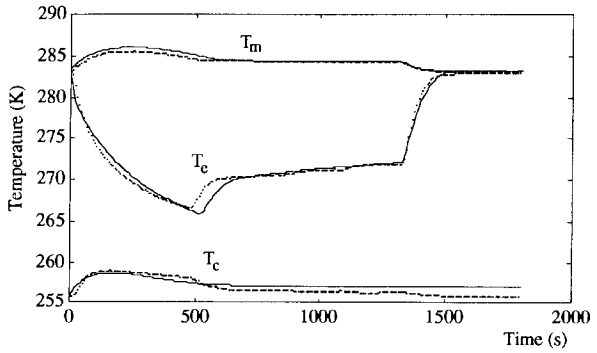

Fig. 17. Experimental (dotted lines) and simulated (continuous lines) behaviour during an isothermal experiment. Initial conditions: 1.6 mol HCl, 41.5 mol H_2O and T_{sp} = 283.2 K; turbine G/L stirrer, 500 rpm, P-control = 10. Additions of NaOH solution at 0.6 gs^{-1} of dosing rate during 35.2 min, 1.4 mol NaOH and 38.0 mol of H_2O.

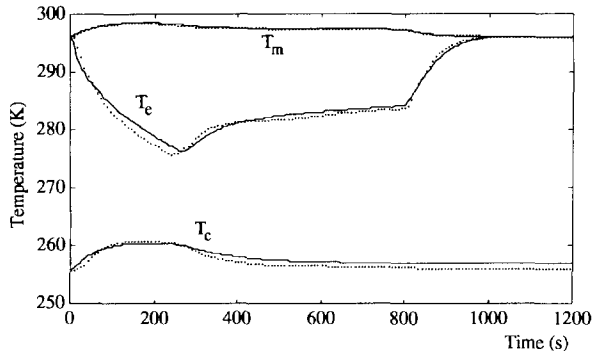

Fig. 18. Experimental (dotted lines) and simulated (continuous lines) behaviour during an isothermal experiment. Initial conditions: 1,8 mol HCl, 45.6 mol H_2O and T_{sp} = 296.2 K; turbine G/L stirrer, 500 rpm, *P*-control = 10. Additions of NaOH solution at 1.2 g s^{-1} of dosing rate during 13.3 min, 1.8 mol NaOH and 49.4 mol of H_2O.

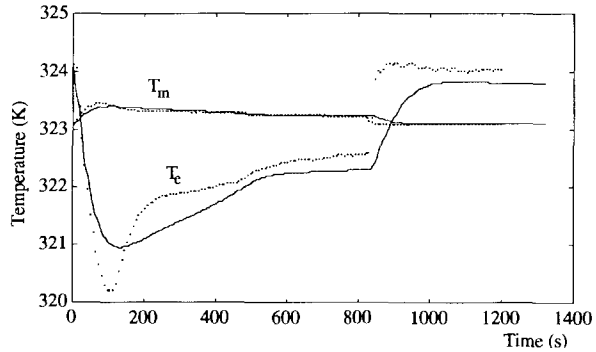

Fig. 19. Experimental (dotted lines) and simulated (continuous lines) behaviour during an isothermal experiment. Initial conditions: 1.6 mol HCl, 41.4 mol H_2O and T_{sp} = 323.2 K; turbine G/L stirrer, 500 rpm, *P*-control = 10. Additions of NaOH solution at 1.0 g s^{-1} of dosing rate during 13.9 min, 1.6 mol NaOH and 44.9 mol of H_2O.

8. Conclusions

The formulated mathematical model adequately describes the significant process behaviour of the reaction calorimeter. The model of the reaction mass with lumped parameters satisfies the level of knowledge of fine chemical processes. The modelisation of heat transfer through the reactor wall, assuming thermal non-homogeneity, is important whenever fast transients take place. Furthermore, to simulate all the thermal operating modes, it has been necessary to model accurately the temperature controller of the reaction calorimeter, including the dynamics of the heating/cooling circuits.

Considerable effort has been devoted to the characterisation of the equipment. Fortunately, only few parameters of the model are specified to the reaction calorimeter

and, therefore, the simulator can easily be applied to other equipment of similar characteristics [10]. Concerning the external cold source, an additional adjustment should be made to calculate the heat removed. Furthermore, it has been observed that the values of the heat transfer coefficient differ between one apparatus and an other and, therefore, should be characterized for each reaction calorimeter. However, following the procedures described in this work, the adjustment of these thermal effects can be easily performed.

One of the most important features of the implementation of this simulator is flexibility from the physico-chemical and thermokinetics viewpoints. The user, according to the data available and his understanding of the process, may define the data complexity, which can vary from very simple, e.g. constant values, to more complex, e.g. temperature and concentration dependences.

The results of the simulator of the reaction calorimeter are, in general, in excellent agreement with the experimental values. The main observed differences are attributable to the lack of appropriate data that frequently are only valid within a short range of process variables. Undoubtedly, the thermo-kinetic data are the most sensitive; for instance, even for a simple reaction such as the neutralisation between sodium hydroxide and hydrogen chloride, the heat of solution is still not well known. Another problem concerns the definition of the mixture properties which usually, in the absence of experimental data, are treated as ideal systems.

Appendix 1: The Mettler RC1 reaction calorimeter

The RC1 is a computer-controlled batch reactor able to carry out isothermal, adiabatic, isoperibolic, and temperature programmed experiments [26].

The stirred glass reactor is surrounded by a jacket in which heat transfer fluid circulates at very high rate. In typical operating conditions, a controller adjusts the temperature of the heat transfer fluid to follow the required temperature programme.

The calorimetric principle implemented in the RC1 is based on the continuous measurement of the temperature difference between the reaction medium and the heat transfer fluid.

The use of a powerful thermostat allows rapid adjustment of the jacket temperature, which is essential to deal with fast transients into the reaction mass.

The main characteristics are:

— Glass reactor of similar geometry to industrial vessels (effective volume 0.5–2 l).
— RD10 dosing controller with two independent control loops for automatic weight and additional inputs and outputs for other measurements (pH, pressure, etc.).
— Stirrer motor with adjustable speed control.
— Temperature working range from −20 to 200°C.

The complete operation of the RC1 is menu-supported and experiments can be run either under direct control or, if preprogrammed, in fully automatic mode, following a recipe introduced beforehand by the operator. During the experiment the values of selected variables can be displayed on the screen and/or plotted, and/or recorded on

a diskette. The information stored allows subsequent evaluation of parameters such as heat of reaction, heat transfer coefficient, heat capacity of reaction mass, etc.

A.1. Reactor characteristics

The main dimensions of the reactor are described in Fig. A1. D_0, D_i, D_a, and D_t are the external, internal, stirrer and hydraulic diameters respectively, and $\mathbf{e}_w$ is the wall thickness.

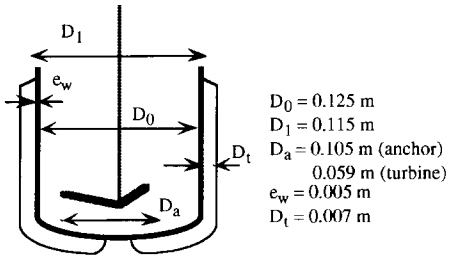

Fig. A1. Dimensions of the standard glass reactor.

The total heat transfer surface, S_T, is equal to $7.47 \times 10^{-2}\,m^2$; the terms $[S_B - 2V_B/R_0]$ (Eq. (28)) is equal to $6.545 \times 10^{-3}\,m^2$. The height of the reactor (Eq. (30) in Section 3). H_T, is equal to 0.193 m, and the total volume (Eq. (53)), V_T, is 21.

The thermal conductivity (λ_W) and specific heat capacity (C_{pw}) of the wall can be correlated using the following expressions

$$\lambda_w = 0.827 + 5.0 \times 10^{-4}(T_m + T_e) \tag{A1}$$

$$C_{pw} = 354.9 + 1.41\,T_w \tag{A2}$$

and the density is $\rho_W = 2600\ kg\,m^{-3}$. The total mass of the glass is 1.11 kg.

A.2. Heat transfer fluid properties

The heat transfer fluid is a silicon oil, Rhodorsil 47V20. The variation of its properties as a function of temperature can be correlated by means of the following expressions

$$\ln \eta_e = 1.5692 \times 10^3 \left(\frac{1}{T_e} - \frac{1}{7.052 \times 10^2} \right) \tag{A3}$$

$$\rho_e = 1.758 \times 10^3 - 4.96\,T_e + 9.8 \times 10^{-3}\,T_e^2 - 7.34 \times 10^{-6}\,T_e^3 \tag{A4}$$

$$C_{pe} = 9.614 \times 10^2 + 1.8\,T_e \tag{A5}$$

$$\lambda_e = 2.205 \times 10^{-1} - 2.33 \times 10^{-4}\,T_e \tag{A6}$$

References

[1] B. Rasmussen, J. Loss Prev.Process Ind., 1 (1988) 92.
[2] W. Regenass, The Protection of Exothermic Reactors and Pressurised Storage Vessels, IChemE Symposium Series, 85 (1984) 1–11.
[3] G.D. Cawthon and K.S. Knaebel, Computer Chem.Eng., 13 (1989) 63.
[4] M.H. Gordon, G.J. O'Brien, C.J. Hensler and K. Marcali, Plant/Operation Progress, 1 (1982) 27.
[5] D. Bonvin, P. de Vallière and D.W.T. Rippin, Computer Chem. Eng., 13 (1989) 1.
[6] R. Reisen and B. Grob, Swiss Chem., 7 (1985) 39.
[7] F. Strozzi,M.A. Alós and J.M. Zaldívar, Chem. Eng. Sci., 49 (1994) 5549.
[8] H. Hernández, J.M. Zaldívar and C. Barcons, Computer Chem. Eng., 17S (1993) 45.
[9] J.M. Zaldívar, C. Barcons, H. Hernández, E. Molga and T.J. Snee, Chem. Eng. Sci., 47 (1992) 2517.
[10] J.M. Zaldívar, H. Hernández, H.Nieman, E. Molga and C. Bassani, J. Loss Prev. Process Ind., 6 (1993) 319.
[11] J.M. Zaldívar, M.A. Alós, E. Molga, H. Hernández and K.R. Westerterp, Chem. Eng. Proc., 34 (1995) 529.
[12] J.M. Zaldívar, M.A. Alós, E. Molga, H. Hernández and K.R. Westerterp, Chem. Eng. Proc., 34 (1995) 543.
[13] S.M. Walas, Modeling with Differential Equations in Chemical Engineering, Butterworth-Heinemann, Stoneham, 1991, p. 313–340.
[14] S. Glasstone, Thermodynamics for the Chemist, Van Nostrand Inc., New York, 1947, p. 537–541.
[15] J.M. Zaldívar, H. Hernández, C. Barcons and R. Nomen, J. Therm.Anal., 38 (1992) 2575.
[16] J.P. Euzen, P. Trambouze and J.P. Wauqier, Scale-up Methodology for Chemical Processes, Gulf Publishing Company, Houston, 1993, p. 153.
[17] V.W. Uhl and J.B. Gray (Eds.), Mixing: Theory and Practice, Vol. 1 and 2, Academic Press, New York, 1966, p. 280–295.
[18] F.A. Holland, Fluid flow for Chemical Engineers, Edward Arnold, London, 1973, p. 249–252.
[19] F. Bondy and S. Lippa, Chem.Eng., 4(1983) 62.
[20] L.L. Tavlarides and M. Stamatoudis, The analysis of interphase reactions and mass transfer in liquid–liquid dispersions, in T.B. Drew, G.R. Cokelet, J.W. Hoopes, Jr and T. Vermeulen (Eds.), Advances in Chemical Engineering, Vol 11, Academic Press, New York, 1981, p. 199–266.
[21] J.R. Bourne, M. Buerli and W. Regenass, Chem. Eng. Sci., 36 (1981) 347.
[22] W.H. Press, B.P. Flannery, S.A. Teukolsky and W.T. Vetterling, Numerical Recipies, Cambridge University Press, New York, 1986, p. 294–312.
[23] P. de Vallière and D. Bonvin. On the dynamics of a bench-scale calorimeter. IFAC Control of Distillation Columns and Chemical Reactors, 1986, p. 301–310.
[24] W. Regenass et al., United States patent 4, 456, 386; Jun.26 (1984).
[25] Private communication, Mettler AG, Switzerland.
[26] F. Chenneaux. E. Ohlmer, W. Schultze and I. Van Gerwen, Flow Characterisation of the Mettler Calorimeter RC1 Technical Note No. I.90.46, Joint Research Center of C.E.C., Ispra (Italy), 1990.
[27] O.A. Hougen, K.M. Watson and R.A. Ragatz, Chemical Process Principles, Part I, John Wiley, New York, 1954, p. 268–270.
[28] RC1 Operating Instructions, Mettler AG, Switzerland, 1989.